Available online at www.sciencedirect.com
SCIENCE DIRECT®
Journal of Photochemistry and Photobiology A: Chemistry 171 (2005) 97–106
Journal of Photochemistry and Photobiology A:Chemistry
www.elsevier.com/locate/jphotochem

UV photodegradation of azo dye Diacryl Red X-GRL

Weirong Zhao*, Zhongbiao Wu, Huixiang Shi, Dahui Wang

Department of Environmental Engineering, Zhejiang University, Hangzhou 310027, China

Received 26 March 2004; received in revised form 13 August 2004; accepted 29 September 2004
Available online 11 November 2004

Abstract

The direct UV photodegradation of Diacryl Red X-GRL was studied in an immersion photochemical reactor equipped with monochromatic UV source of 253.7 nm. Different process parameters that may influence the UV photodegradation were studied. These parameters included temperature, pH, radiation flow rate of UV lamp, carrier gas flow rate, initial concentration of dye, concentration of *t*-BuOH, and the concentration of dissolved oxygen. Four possible photodegradation pathways of dye in the presence of dissolved oxygen were assumed to be as follows: homolysis of excited dye to radicals; electron transfer of excited dye to form radical dye cation; decomposition by superoxide radical anion; and decomposition by singlet oxygen. Based on photodegradation pathways the photodegradation rate equation was derived, and the overall quantum yield of photodegradation was determined using Line Source Spherical Emission Model (LSSE Model), which describes the radiation flow rate absorbed by the solution in the photodegradation process. The overall quantum yield is enhanced enormously from 0.46×10^{-3} in the absence of dissolved oxygen to 7.35×10^{-3} in the presence of 1.21×10^{-3} M dissolved oxygen. However, the temperature had negative effect on the overall quantum yield, which varied from 8.54×10^{-3} at 288 K to 5.53×10^{-3} at 308 K. Finally, by using non-linear regression analysis, the overall quantum yield was correlated to be a function of temperature and dissolved oxygen in a modified Arrhenius equation with activation energy of 11.3 kJ mol^{-1}.

Keywords: Diacryl Red X-GRL; Azo dye; Overall quantum yield; Photodegradation; Kinetics

1. Introduction

Textile industries have shown a significant increase in the use of synthetic complex organic dyes as the coloring material. The annual world production of textiles is about 30 million tones requiring 0.7 million tones of different dyes per year [1]. Among these dyes, over 50% are azo dyes. About 10–20% of the dyes utilized is lost in the process effluent, resulting in great volumes of highly colored effluents [2–4].

Usually, the conventional biological treatment processes do not readily remove dyes from textile wastewaters, because of their resistance to biological degradation [5–7]. Although some treatment processes, like chemical coagulation and active carbon adsorption, may remove certain categories of dye to about 90%, the main drawback of these processes is the generation of a large amount of sludge or solid waste, resulting in high operational costs for sludge treatment and disposal [8,9].

The photodegradation, which has the advantage of neither chemical sludge nor toxic residue left out in the treatment processes [10], is very suitable for colored wastewater treatment. Therefore, it is meaningful to study the behavior of dyes in aqueous solution during UV using kinetics data. Diacryl Red X-GRL selected for this study is an azo dye broadly used in the textile industry, and is nonbiodegradable by the conventional activated sludge process [11].

In the present work, the photodegradation of Diacryl Red X-GRL was studied to determine the impact of operating conditions. The possible photodegradation pathways of dye in the presence of dissolved oxygen were assumed. Using Line Source Spherical Emission Model (LSSE Model), the overall quantum yield of reaction was obtained by applying

* Corresponding author. Tel.: +86 571 8795 1239; fax: +86 571 8795 2771.
E-mail address: weirong@mail.hz.zj.cn (W. Zhao).

1010-6030/$ – see front matter © 2004 Elsevier B.V. All rights reserved.
doi:10.1016/j.jphotochem.2004.09.013

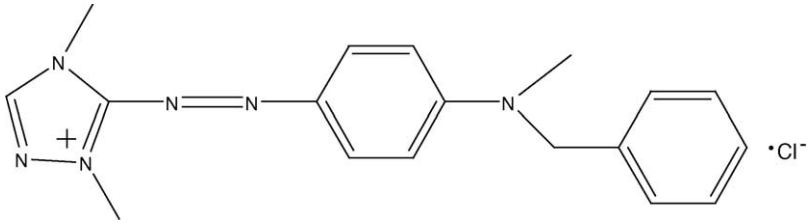

Fig. 1. Structural formula of Diacryl Red X-GRL.

the experimental data to a kinetics model. Finally, the overall quantum yield was expressed as a function of temperature and dissolved oxygen in a modified Arrhenius equation by non-linear regression analysis.

2. Experimental

2.1. Reagents

Water was deionized and distilled. The commercial azo dye Diacryl Red X-GRL, 5-[4-(benzyl-methyl-amino)-phenylazo]-1,4-dimethyl-4*H*-[1,2,4]triazol-1-ium chloride, was purified by methanol recrystallization method [11]. As can be seen in Fig. 1, its cation part connects with a chloride ion by ionic bond. The molecular weight of dye is 356.84 g mol^{-1}, and its maximum absorbance wavelength is at 530 nm with molar extinction coefficient of 4.57×10^4 M^{-1} cm^{-1}. The carrier gas was either pure oxygen (>99.5%), or pure nitrogen (99.99%), or the mixture of both in certain volumetric proportions.

2.2. Apparatus

Photodegradation studies were conducted in a 3.5 L immersion photochemical Pyrex glass reactor as described in our previous work [11]. The structure and dimensions of the reactor are depicted in Fig. 2. The reactor was submerged in a thermostatic bath to keep the temperature within ±05 °C of the desired value. The reactor was equipped with a few inlets for bubbling the carrier gas, sampling, venting, and temperature measurement. The low-pressure mercury vapor lamp (Zuozhou Light Source Co., Hebei, China) used was situated in a quartz sleeve emitting monochromatic light of 253.7 nm. The procedure for the calculation of the radiation flow rate $P_{253.7}$ emitted by the lamp of 10 and 30 W using are presented in the appendix. Results obtained from these calculations show that $P_{253.7}$ for 30 and 10 W is $(4.47 \pm 0.17) \times 10^{-6}$ and $(2.40 \pm 0.13) \times 10^{-6}$ Einstein s^{-1}, respectively.

2.3. Analytical methods

For all the experiments, the reactor was filled with 3.5 L of aqueous Diacryl Red X-GRL buffer solution adjusted with orthophosphoric acid and sodium hydroxide to achieve the desired pH and ionic strength of 0.1 M. During the process, several samples were taken out from the reactor periodically to analyze the absorbance of the solution by UV–vis spectrophotometer (Pgenral Analytical Instrument Co. Ltd., Beijing, China) at 253.7 and 530 nm respectively. The concentration of Diacryl Red X-GRL was determined at maximum absorbance wavelength of 530 nm by Beer–Lambert's law [12]. The attenuation coefficient μ_D of the solution at 253.7 nm was calculated by dividing the absorbance of solutions at 253.7 nm by the light path length (0.01 m).

3. Results and discussion

3.1. Influence of reaction variables

The photodegradation of Diacryl Red X-GRL by monochromatic UV radiation was carried out in the experiments by varying process conditions according to the values

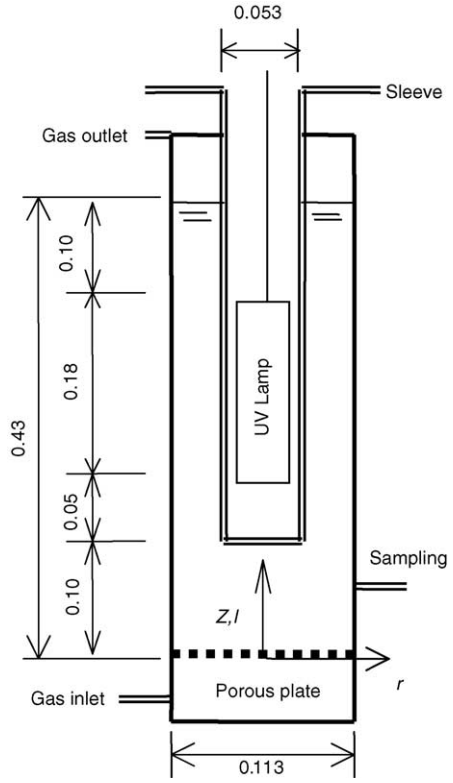

Fig. 2. Experimental apparatus (unit: m).

Table 1
Experimental results for photodegradation of Diacryl Red X-GRL

Exp.	T (K)	pH	$P_{253.7} \times 10^6$ (Einstein s^{-1})	$C_{D,0} \times 10^5$(M)	Q_{gas} (L h^{-1})	$C_{oxygen} \times 10^3$ (M)	$C_{t\text{-BuOH}} \times 10^3$ (M)	$\phi_D \times 10^3$
UV-1	298	3.15	4.47	1.34	100	1.21	0	6.72
UV-2	298	5.70	4.47	1.34	100	1.21	0	7.11
UV-3	298	8.14	4.47	1.35	100	1.21	0	7.35
UV-4	298	9.24	4.47	1.47	100	1.21	0	7.56
UV-5	288	5.70	4.47	1.40	100	1.45	0	8.54
UV-6	293	5.70	4.47	1.47	100	1.32	0	7.77
UV-7	303	5.70	4.47	1.33	100	1.12	0	6.16
UV-8	308	5.70	4.47	1.33	100	1.05	0	5.53
UV-9	298	8.14	4.47	1.36	40	1.21	0	7.28
UV-10	298	8.14	4.47	1.36	100	0	0	0.46
UV-11	298	8.14	4.47	1.36	100	0.24	0	1.54
UV-12	298	8.14	4.47	1.36	100	0.48	0	2.63
UV-13	298	8.14	4.47	1.36	100	0.73	0	3.78
UV-14	298	8.14	4.47	1.36	100	0.97	0	4.80
UV-15	298	3.15	4.47	2.80	100	1.21	0	6.65
UV-16	298	8.14	2.40	1.39	100	1.21	0	7.42
UV-17	298	8.14	4.47	1.36	100	1.21	20	/
UV-18	298	8.14	4.47	1.36	100	1.21	50	/

shown in Table 1. The process variables include temperature T, pH, carrier gas flow rate Q_{gas}, radiation flow rate of UV lamp $P_{253.7}$, concentration of t-BuOH $C_{t\text{-BuOH}}$, initial concentration of dye $C_{D,0}$ and concentration of dissolved oxygen C_{oxygen}. In Table 1 the concentration of the dissolved oxygen was taken from Perry and Green [13]. The influence of variables on the conversion of dye is depicted in Fig. 3.

As shown in Fig. 3a, the concentration of the dissolved oxygen influenced the process significantly. At the reaction time of 360 min and carrier gas flow rate of 100 L h^{-1}, the conversion of dye increased with increasing concentration of dissolved oxygen. The conversion of dye increased to 0.716 with dissolved oxygen of 1.21×10^{-3} M when compared to the conversion of 0.090 without any dissolved oxygen. Therefore, it could be concluded that the dissolved oxygen took part in photodegradation process.

Fig. 3a showed that the oxygen flow rate had limited effect on the conversion of dye, as the reaction was not diffusion determined.

When the reaction time was 360 min, the conversion of dye increased with radiation flow rate of UV lamp $P_{253.7}$ from 0.598 at 2.40×10^{-6} Einstein s^{-1} to 0.716 at 4.47×10^{-6} Einstein s^{-1}, as shown in Fig. 3b, because the radiation flow rate absorbed by the solution increased with the radiation flow rate of UV lamp.

It can be inferred from Fig. 3c that the conversion of dye increased with the decrease of dye initial concentration. However, this conclusion could be misleading. The initial photodegradation rate of dye calculated from the slope of the curves were 7.04×10^{-10} and 9.99×10^{-10} M s^{-1} when the initial concentrations were 1.36×10^{-5} and 2.80×10^{-5} M, respectively. This implied that the reaction rate increased with the initial concentration. For photochemical reactions, the high concentration caused a high light absorption and consequently an increase of reaction rate.

Fig. 3d shows that the pH had no influence on the photodegradation since the process is not influenced by H^+/OH^- (see Section 3.2).

Temperature had negative influence on the conversion of dye, as shown in Fig. 3e. At the reaction time of 360 min, the conversion of dye decreased from 0.748 to 0.594 as temperature was increased from 288 to 308 K. From Table 1, it can be observed that the concentration of dissolved oxygen decreased with increasing of temperature, which in turn decreased the photodegradation rate. Therefore, under the strong influence of the concentration of dissolved oxygen, the conversion of dye was reduced when temperature increased.

The study of photodegradation with the addition of t-BuOH known as a radical scavenger was used to find out the dominant reaction in the degradation process [14]. Fig. 3f presented the alteration of the conversion of dye during the reaction for various t-BuOH concentrations. The conversion of dye decreased from 0.716 without t-BuOH to 0.530 and 0.454 with t-BuOH of 20×10^{-3} and 50×10^{-3} M, respectively. Thus, it can be deduced that the photodegradation process might be dominated by radical reaction.

3.2. Mechanism study

The mechanism for photochemical reactions of organic compounds in the presence of dissolved oxygen is usually complex, as reported by Legrini et al. [14] and Aranyosi et al. [15]. Usually, the UV light-induced photodegradation of dyes in the presence of dissolved oxygen can be achieved by the cleavage of conjugated chains that will shift the absorbance spectra out of visible region [5]. It has been reported that the superoxide radical anion $O_2^{\bullet -}$ can be generated when UV is absorbed by dissolved oxygen [16]. Yang et al. [17] also proved that the superoxide radical anion might be the

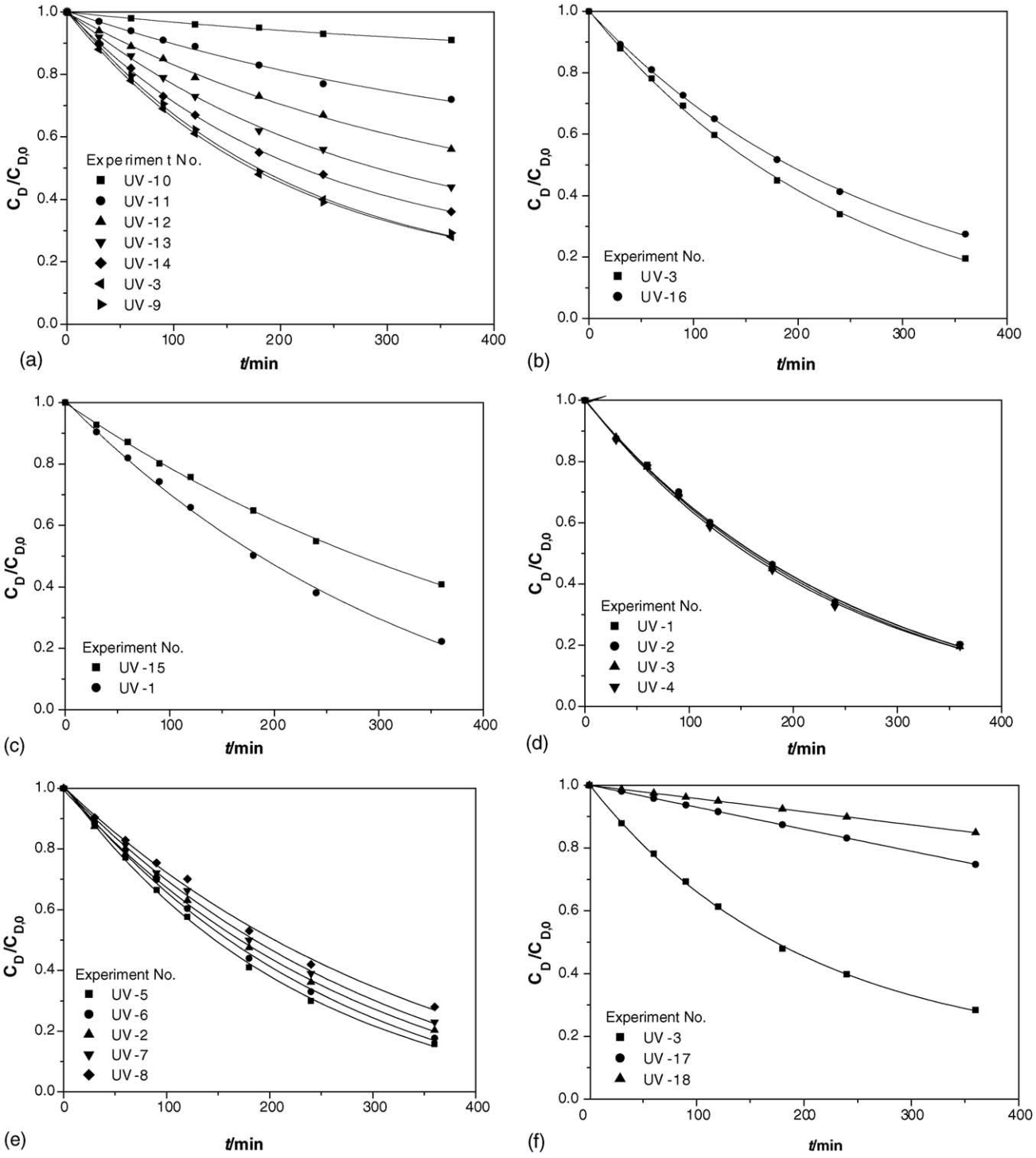

Fig. 3. Influence of variables on conversion of Diacryl Red X-GRL (experimental conditions are listed in Table 1). (a) Carrier gas flow rates and concentrations of dissolved oxygen. (b) Radiation flow rates of UV lamp. (c) Initial concentrations of dye. (d) pH. (e) Temperatures. (f) Concentrations of *t*-BuOH.

key radical in the photodegradation. The formation pathways and overall quantum yield of singlet oxygen $^1O_2$, a powerful oxidant, has been reviewed extensively by Wilkinson et al. [18].

Based on experimental results of reaction variables and photochemistry principles, a mechanism for Diacryl Red X-GRL photodegradation is proposed.

In a first step, the excitation of the Diacryl Red X-GRL, represented by D, takes place by the absorption of one photon:

$$D + h\nu \xrightarrow{\phi'_D \mu_D I} D^* \quad (1)$$

where ϕ'_D being the overall quantum yield of dye from its ground state to excitation state, μ_D (m^{-1}) and I (Ein-

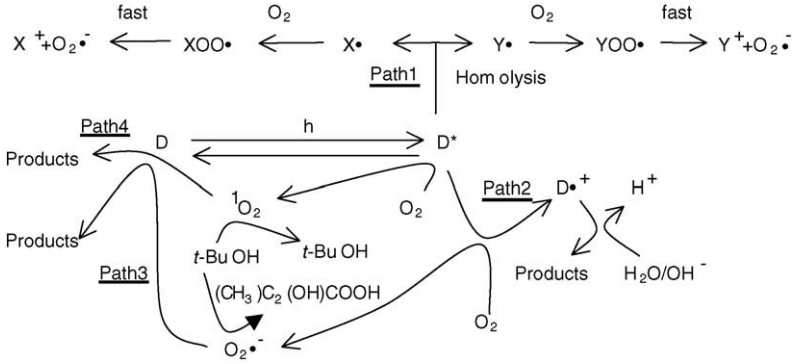

Fig. 4. Scheme of Diacryl Red X-GRL photodegradation pathways.

stein s^{-1} m^{-2}) being the attenuation coefficient of the solution and the radiation intensity, respectively, for 253.7 nm of monochromatic radiation. The excited dye D^* is later deactivated to its ground state:

$$D^* \xrightarrow{k_1} D \quad (2)$$

or can be decomposed by homolytic cleavage to radicals ($X^\bullet$ and $Y^\bullet$) that then react with dissolved oxygen to form $XOO^\bullet$ and $YOO^\bullet$, while the $XOO^\bullet$ and $YOO^\bullet$ are decomposed to X^+, Y^+ and $O_2{}^{\bullet -}$ quickly [19]:

$$D^* \xrightarrow{k_2} X^\bullet + Y^\bullet \quad (3)$$

$$X^\bullet + O_2 \xrightarrow{k_3} XOO^\bullet \xrightarrow{\text{fast}} X^+ + O^\bullet{}_2{}^- \quad (4)$$

$$Y^\bullet + O_2 \xrightarrow{k_4} YOO^\bullet \xrightarrow{\text{fast}} Y^+ + O^\bullet{}_2{}^- \quad (5)$$

The excited dye D^* transfers an electron to a ground state molecular oxygen, forming a radical dye cation $D^{\bullet +}$ and a superoxide radical anion $O_2{}^{\bullet -}$ as shown in Eq. (6) [14]. The superoxide radical anion further reacts with dye (Eq. (7)) and the radical dye cation is hydrolyzed (Eq. (8)).

$$D^* + O_2 \xrightarrow{k_5} D^{\bullet +} + O_2{}^{\bullet -} \quad (6)$$

$$D + O_2{}^{\bullet -} \xrightarrow{k_6} \text{Products} \quad (7)$$

$$D^{\bullet +} + H_2O \xrightarrow{k_7} \text{Products} + OH^- \quad (8)$$

The excited dye D^* transfers energy to a ground state molecular oxygen, forming a ground state dye D and a singlet oxygen $^1O_2$ as shown in Eq. (9). The singlet oxygen reacts with the dye further (Eq. (10)) [20]:

$$D^* + O_2 \xrightarrow{k_8} D + {}^1O_2 \quad (9)$$

$$D + {}^1O_2 \xrightarrow{k_9} O_2 + \text{Products} \quad (10)$$

Radical scavenger such as *t*-BuOH reacts with superoxide radical anion $O_2{}^{\bullet -}$ (Eq. (11)), and then inhibits the reaction rate between D and $O_2{}^{\bullet -}$ [19]:

$$t\text{-BuOH} + O_2{}^{\bullet -} + H_2O \xrightarrow{k_{10}} O_2 + (CH_3)_2C(OH)COOH + OH^- \quad (11)$$

The *t*-BuOH can quench the singlet oxygen $^1O_2$ (Eq. (12)):

$$t\text{-BuOH} + {}^1O_2 \xrightarrow{k_{11}} O_2 + t\text{-BuOH} \quad (12)$$

The radicals formed from the above reactions are terminated as follows:

$$X^\bullet + X^\bullet \xrightarrow{k_{12}} X - X \quad (13)$$

$$Y^\bullet + Y^\bullet \xrightarrow{k_{13}} Y - Y \quad (14)$$

$$X^\bullet + Y^\bullet \xrightarrow{k_{14}} D \quad (15)$$

$$X^\bullet + O_2{}^{\bullet -} \xrightarrow{k_{15}} XO_2{}^- \quad (16)$$

$$Y^\bullet + O_2{}^{\bullet -} \xrightarrow{k_{16}} YO_2{}^- \quad (17)$$

As the radical reactions are non-selective and diffusion controlled, the second-order rate constant of the reaction between organic substrates and the radicals is very close to that of the reaction between the radicals (both at the magnitude of 10^8–10^{10} M^{-1} s^{-1}) [21–23]. Therefore, it is reasonable to assume that the concentration of various radicals is much lower than the concentration of dye and dissolved oxygen. Comparing the radical consumption rates of Eqs. (4), (5) and (7), the radical consumption rates of Eqs. (13)–(17) are negligible, and hence, the Eqs. (13)–(17) were ignored in the following study.

Summarizing the above results of Eqs. (1)–(12), the possible photodegradation pathways of dye under the UV radiation of 253.7 nm in the presence of dissolved oxygen can be assumed to be that depicted in Fig. 4. As can be seen from Fig. 4, there are four photodegradation pathways for the dye. The first pathway is the homolysis of excited dye (Path1) to radicals $X^\bullet$ and $Y^\bullet$, which then react with dissolved oxygen to form $XOO^\bullet$ and $YOO^\bullet$, while the $XOO^\bullet$ and $YOO^\bullet$ decompose to X^+, Y^+ and $O_2{}^{\bullet -}$ quickly. The second pathway involves the transfer of an electron from the excited dye to

ground state molecular oxygen (Path2) to form a superoxide radical anion $O_2^{\bullet-}$ and a radical dye cation. The third pathway is the decomposition of dye by superoxide radical anion (Path3). The fourth pathway is that an excited dye transfers its energy to ground state molecular oxygen, forming a ground state dye D and a singlet oxygen $^1O_2$, while the singlet oxygen reacts with the dye further (Path4).

3.3. Kinetics study

According to Fig. 4 and Eqs. (1)–(12), the kinetics equation of D, D^*, $O_2^{\bullet-}$, $^1O_2$, $X^\bullet$, and $Y^\bullet$ can be deduced as follows:

$$\frac{dC_D}{dt} = -\phi'_D\mu_D I + k_1 C_{D^*} - k_6 C_D C_{O_2^{\bullet-}} + k_8 C_{D^*} C_{oxygen} - k_9 C_D C_{^1O_2} \quad (18)$$

$$\frac{dC_{D^*}}{dt} = \phi'_D\mu_D I - k_1 C_{D^*} - k_2 C_{D^*} - k_5 C_{D^*} C_{oxygen} - k_8 C_{D^*} C_{oxygen} \quad (19)$$

$$\frac{dC_{O_2^{\bullet-}}}{dt} = k_5 C_{D^*} C_{oxygen} - k_6 C_D C_{O_2^{\bullet-}} + k_3 C_{X^\bullet} C_{oxygen} + k_4 C_{Y^\bullet} C_{oxygen} - k_{10} C_{O_2^{\bullet-}} C_{t\text{-BuOH}} \quad (20)$$

$$\frac{dC_{^1O_2}}{dt} = k_8 C_{D^*} C_{oxygen} - k_9 C_D C_{^1O_2} - k_{11} C_{^1O_2} C_{t\text{-BuOH}} \quad (21)$$

$$\frac{dC_{X^\bullet}}{dt} = k_2 C_{D^*} - k_3 C_{X^\bullet} C_{oxygen} \quad (22)$$

$$\frac{dC_{Y^\bullet}}{dt} = k_2 C_{D^*} - k_4 C_{Y^\bullet} C_{oxygen} \quad (23)$$

Applying the steady state assumption to the concentration of excited dye D^* (Eq. (19)), superoxide radical anion $O_2^{\bullet-}$ (Eq. (20)), singlet oxygen $^1O_2$ (Eq. (21)), radicals $X^\bullet$ (Eq. (22)) and $Y^\bullet$ (Eq. (23)) yields the following equations:

$$C_{D^*} = \phi'_D\mu_D I \frac{\begin{array}{r} k_6 C_D(k_5 C_{oxygen} + 2k_2/k_6 C_D + k_{10} C_{t\text{-BuOH}}) \\ +(k_9 C_D k_8 C_{oxygen}/k_9 C_D + k_{11} C_{t\text{-BuOH}}) \\ +k_5 C_{oxygen} + k_2 \end{array}}{k_1 + k_2 + k_5 C_{oxygen} + k_8 C_{oxygen}} \quad (24)$$

$$C_{O_2^{\bullet-}} = \frac{(k_5 C_{oxygen} + 2k_2) C_{D^*}}{k_6 C_D + k_{10} C_{t\text{-BuOH}}} \quad (25)$$

$$C_{^1O_2} = \frac{k_8 C_{D^*} C_{oxygen}}{k_9 C_D + k_{11} C_{t\text{-BuOH}}} \quad (26)$$

$$C_{X^\bullet} = \frac{k_2 C_{D^*}}{k_3 C_{oxygen}} \quad (27)$$

$$C_{Y^\bullet} = \frac{k_2 C_{D^*}}{k_4 C_{oxygen}} \quad (28)$$

Substituting Eqs. (24)–(26) into Eq. (18) leads to:

$$-r_D = -\frac{dC_D}{dt} = \phi'_D \left[\frac{\begin{array}{r} k_6 C_D(k_5 C_{oxygen} + 2k_2/k_6 C_D + k_{10} C_{t\text{-BuOH}}) \\ +(k_9 C_D k_8 C_{oxygen}/k_9 C_D + k_{11} C_{t\text{-BuOH}}) \\ +k_5 C_{oxygen} + k_2 \end{array}}{k_1 + k_2 + k_5 C_{oxygen} + k_8 C_{oxygen}} \right] \times \mu_D I \quad (29)$$

The overall quantum yield $\phi_{D,t\text{-BuOH}}$ in the presence of *t*-BuOH is defined by the expression below:

$$\phi_{D,t\text{-BuOH}} = \phi'_D \left[\frac{\begin{array}{r} k_6 C_D(k_5 C_{oxygen} + 2k_2/k_6 C_D + k_{10} C_{t\text{-BuOH}}) \\ +(k_9 C_D k_8 C_{oxygen}/k_9 C_D + k_{11} C_{t\text{-BuOH}}) \\ +k_5 C_{oxygen} + k_2 \end{array}}{k_1 + k_2 + k_5 C_{oxygen} + k_8 C_{oxygen}} \right] \quad (30)$$

As it can be deduced from Eq. (30), the $\phi_{D,t\text{-BuOH}}$ is the function of ϕ'_D, k_1, k_2, k_5, k_6, k_8, k_9, k_{10}, k_{11}, $C_{t\text{-BuOH}}$, C_D, and C_{oxygen}.

If there is no *t*-BuOH present in aqueous solution, the Eq. (30) is simplified to

$$\phi_D = \phi'_D \left[\frac{2k_5 C_{oxygen} + k_8 C_{oxygen} + 3k_2}{k_1 + k_2 + k_5 C_{oxygen} + k_8 C_{oxygen}} \right] \quad (31)$$

As it can be deduced from Eq. (31), the overall quantum yield ϕ_D in the absence of *t*-BuOH is the function of ϕ'_D, k_1, k_2, k_5, k_8, and C_{oxygen}.

Introducing Eq. (31) into Eq. (29) results in:

$$-r_D = -\frac{dC_D}{dt} = \phi_D\mu_D I \quad (32)$$

where $-r_D$ is the conversion rate of dye at certain point of the reactor.

The above reaction equation for certain points of the reactor can be extended to the whole reactor:

$$-r_{D,total} = -\left.\frac{dC_D}{dt}\right|_V = -\frac{1}{V}\int_V r_D dV = \frac{\phi_D}{V}\int_V \mu_D I dV \quad (33)$$

Table 2
Determination of the integration of W_{abs} with t for experimental set UV-3

t (min)	$C_D \times 10^5$ (M)	μ_D (m^{-1})	ω (m^2)	$W_{abs} \times 10^7$ (Einstein s^{-1})	$\int_0^t W_{abs} dt \times 10^4$ (Einstein)
0	1.35	2.61	0.0138	4.47	0
30	1.19	2.41	0.0140	4.19	8.04
60	1.06	2.02	0.0140	3.52	15.10
90	0.94	1.60	0.0140	2.78	20.70
120	0.83	1.45	0.0141	2.54	25.10
180	0.65	1.10	0.0141	1.93	34.60
240	0.54	0.64	0.0142	1.13	39.00
360	0.38	0.58	0.0142	1.03	46.40

where $-r_{D,\ total}$ is the conversion rate of dye of the whole reactor.

In a photochemical reaction promoted by a monochromatic radiation source similar to the current study, the total radiation flow rate absorbed, W_{abs} (Einstein s^{-1}) is given by the expression:

$$W_{abs} = \int_V \mu_D I dV \tag{34}$$

Combining Eqs. (33) and (34) yields:

$$-\frac{dC_D}{dt} = \frac{\phi_D W_{abs}}{V} \tag{35}$$

with the boundary condition:

$$t = 0, \qquad C_D = C_{D,0} \tag{36}$$

Integrating Eq. (35) with the boundary condition (Eq. (36)) gives:

$$C_{D,0} - C_D = \frac{\phi_D}{V} \int_0^t W_{abs} dt \tag{37}$$

According to the above equation, the overall quantum yield of the reaction can be obtained from the slope of the plot of ($C_{D,0}$–C_D) versus integration of W_{abs} with t. The rate of radiation energy absorbed by the solution W_{abs} in Eq. (37) can be determined beforehand by solving a radiation energy balance using a radiation source model that describes the distribution of radiant energy within the reactor. Based on the geometric characteristics of the reactor and the lamp used, the Line Source Spherical Emission Model [24] is found to be suitable and chosen for this study. Basically, the LSSE Model assumes the lamp as an assembly of source points, from which each point emits radiation in all direction isotropically. This model allowed a reasonably good analysis of the radiation energy distribution within the reaction space with an objective to predict the radiation field in a cylindrical annular reactor with the source placed at its axis.

According to the LSSE Model, the radiation flow rate absorbed can be expressed in this form:

$$W_{abs} = 2\pi\mu_D \int_0^H \int_{R_1}^{R_0} I(r, z) r\, dr\, dz \tag{38}$$

where $I(r, z)$ represents the radiation intensity distribution in cylindrical coordinates, which is given by:

$$I(r, z) = \frac{P_{253.7}}{4\pi L} \int_{L_0}^{L_0+L} \frac{\exp[-\mu_D (r - R_1)\sqrt{r^2 + (z - l)^2}/r]}{r^2 + (z - l)^2} dl \tag{39}$$

In Eqs. (38) and (39), r and z are the coordinates of the general point considered, and l is the lamp axial coordinate; L, 0.180 m, and L_0, 0.150 m, are the length and axial position of the lamp; R_1, 0.026 m, and R_0, 0.056 m, are the internal and external radii of the reactor; H, 0.430 m, is the depth of solution in reactor, and $P_{253.7}$ is the radiation flow rate of UV lamp, as determined previously (see appendix).

Substituting Eq. (39) into Eq. (38) using a general parameter ω as defined in the form:

$$\omega = \int_0^H \int_{R_1}^{R_0} \int_{L_0}^{L_0+L} \frac{\exp[-\mu_D (r - R_1)\sqrt{r^2 + (z - l)^2}/r]}{r^2 + (z - l)^2} r\, dl\, dr\, dz \tag{40}$$

Therefore, a reduced equation for the total absorption flow rate was obtained, and can be written as follows:

$$W_{abs} = \frac{P_{253.7}\mu_D\omega}{2L} \tag{41}$$

The μ_D values are experimentally determined and the parameter ω in Eq. (40) can be solved numerically. Once μ_D, ω, and $P_{253.7}$ are known, Eq. (41) allows the determination of W_{abs} for each reaction time and the integration of W_{abs} with t can be performed. As an example, Table 2 shows the calculation for the experiment UV-3 carried out at 298 K and pH 8.14, where the W_{abs} decreases with reaction time.

Fig. 5 shows the temporal integration of W_{abs} versus ($C_{D,0}$–C_D) with various operating conditions. The ϕ_D values of the experiments obtained from Fig. 5 were tabulated in Table 1. As shown in Fig. 5, the straight line is a good fit to the data points, indicating that the kinetics model derived from the proposed photodegradation mechanism is reasonable.

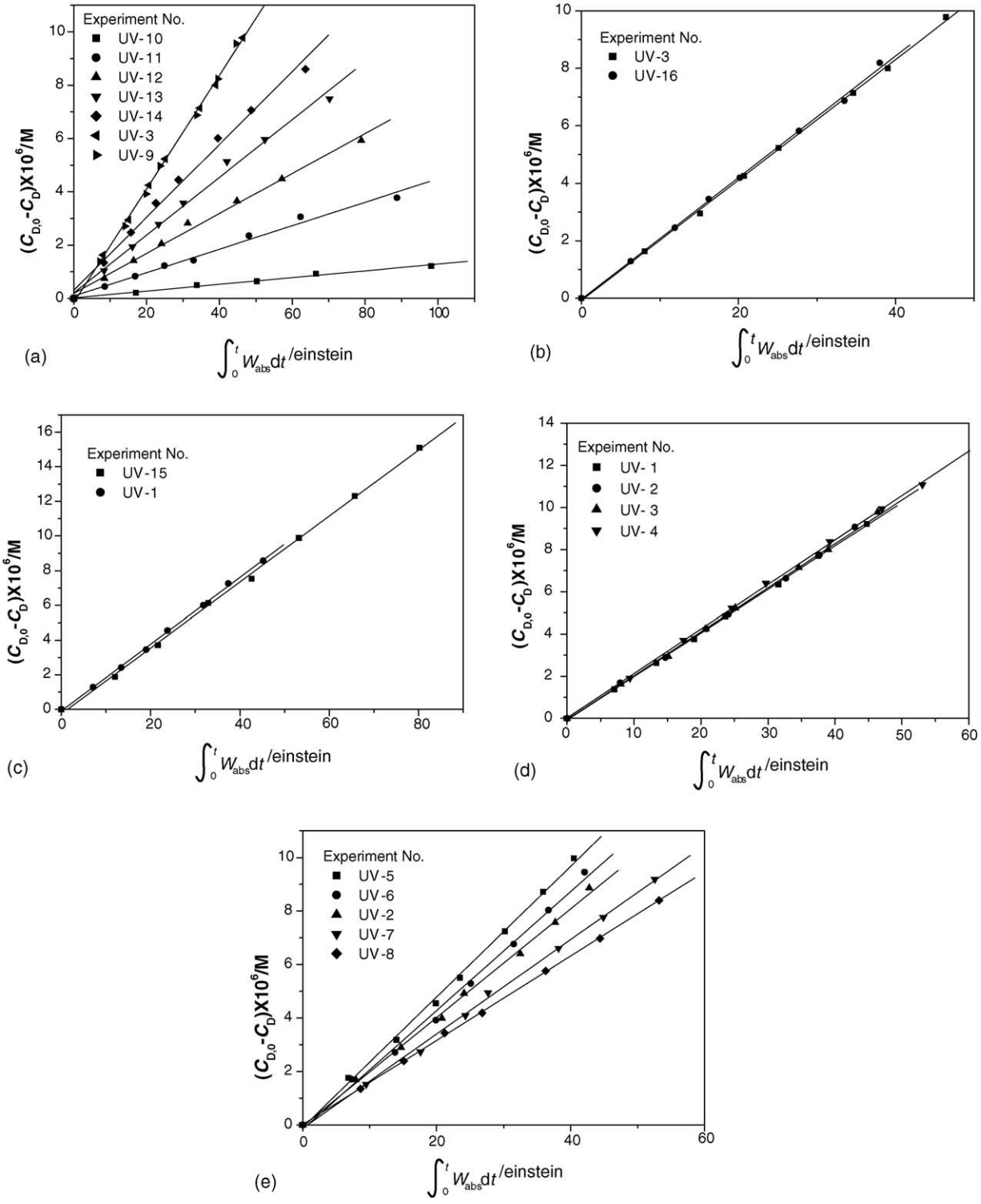

Fig. 5. Determination of the overall quantum yields ϕ_D with variation in (experimental conditions are listed in Table 1). (a) Carrier gas flow rates, and concentrations of dissolved oxygen. (b) Radiation flow rates of UV lamp. (c) Initial concentrations of dye. (d) pHs. (e) Temperatures.

Fig. 5a shows that the dissolved oxygen has significant impact on the quantum yield, which varied from 0.46×10^{-3} without dissolved oxygen to 1.54×10^{-3} and 7.35×10^{-3} with dissolved oxygen of 0.24×10^{-3} and 1.21×10^{-3} M, respectively. On the contrary, the oxygen flow rate did not show any impact on the overall quantum yield.

From Fig. 5b–d, it can be inferred that the radiation flow rate of UV lamp, the initial concentration of dye, and pH are independent of overall quantum yield (Eq. (31)).

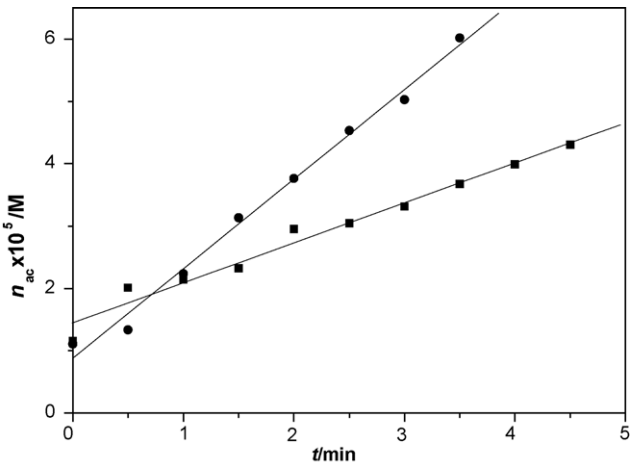

Fig. 6. The plot of n_{ac} vs. t (■) Lamp = 10 W. (●) Lamp = 30 W.

The concentration of dissolved oxygen decreases with the increasing temperature as shown in Table 1. Fig. 5e also shows that the temperature has negative effect on the overall quantum yield, which varies from 8.54×10^{-3} at 288 K to 5.53×10^{-3} at 308 K.

Summarizing the above results, the overall quantum yield in the absence of *t*-BuOH is a function of temperature and concentration of dissolved oxygen. Therefore, after non-linear regression analysis, the overall quantum yields of UV-1–UV-16 in Table 1 can be correlated to a function of the temperature and concentration of dissolved oxygen in a modified Arrhenius expression:

$$\phi_D = \phi_0 \exp\left(\frac{-E_a}{RT}\right) \exp(\xi C_{oxygen})$$

$$= 7.36 \times 10^{-2} \exp\left(\frac{-11298}{RT}\right) \exp(1850 C_{oxygen}),$$

$$r = 0.9693 \quad (42)$$

which E_a being the activation energy of photodegradation, 11.3 kJ mol^{-1}.

4. Conclusion

There are four possible photodegradation pathways of Diacryl Red X-GRL under the UV radiation of 253.7 nm in the presence of dissolved oxygen: homolysis of excited dye to radicals; electron transfer of excited dye to form radical dye cation; decomposition by superoxide radical anion; and decomposition by singlet oxygen.

The photodegradation of dye by UV is strongly dependent on temperature, radiation flow rate of UV lamp, and concentrations of dissolved oxygen and *t*-BuOH. The overall quantum yield is enhanced enormously from 0.46×10^{-3} in the absence of dissolved oxygen to 7.35×10^{-3} in the presence of dissolved oxygen of 1.21×10^{-3} M. However, the temperature has negative effect on the overall quantum yield, which varied from 8.54×10^{-3} at 288 K to 5.53×10^{-3} at 308 K.

The overall quantum yield correlation is a function of the temperature and dissolved oxygen in a modified Arrhenius expression with activation energy of 11.3 kJ mol^{-1} as

$$\phi_D = \phi_0 \exp\left(\frac{-E_a}{RT}\right) \exp(\xi C_{oxygen})$$

$$= 7.36 \times 10^{-2} \exp\left(\frac{-11298}{RT}\right) \exp(1850 C_{oxygen})$$

The experimental results prove that the proposed photodegradation mechanism and the kinetics model are appropriate and reasonable.

Appendix A

In this study, the potassium ferrioxalate actinometry was used to determine the radiation flow rate of lamp $P_{253.7}$ [12]. The overall photochemical reaction of the potassium ferrioxalate, which has the overall quantum yield $\phi_{ac,253.7}$ of 1.25 at 253.7 nm consists of the reduction of ferric ions to ferrous ions:

$$2Fe^{3+} + C_2O_4^{2-} \xrightarrow{253.7nm} 2Fe^{2+} + 2CO_2 \quad (A.1)$$

A series of experiments were performed at pH 1, with the initial concentration of potassium ferrioxalate of 6×10^{-3} M. The quantity of ferrous ions formed during the radiation period was determined spectrophotometrically by measuring the absorbance at 510 nm for the complex formed between these ions and 1,10-phenantroline. The original ferric ions are weakly complexed by 1,10-phenantroline, and therefore will not absorb at 510 nm. This analytical method is very sensitive because the molar extinction coefficient of the ferrous complex at 510 nm is 1.11×10^4 M^{-1} cm^{-1}.

The number of ferrous ions n_{ac} formed during the irradiation period t was determined from the slope of n_{ac} versus t as plotted in Fig. 6. The number of photons of wavelength of 253.7 nm $N_{ac,253.7}$ absorbed during the same period can be calculated using n_{ac} and the overall quantum yield $\phi_{ac,253.7}$ as,

$$N_{ac,253.7} = \frac{n_{ac}}{\phi_{ac,253.7}} \quad (A.2)$$

As the reaction (A.1) is a simple reaction, and ferrioxalate is the only substance which absorbs at the wavelength of 253.7 nm, then application of Beer–Lambert's law [12], provides:

$$P_{ac,253.7} = P_{253.7}(1 - 10^{-A_{ac,253.7}}) \quad (A.3)$$

where $P_{253.7}$ being the radiation flow rate of UV lamp at wavelength of 253.7 nm, Einstein s^{-1}; $P_{ac,253.7}$ being the rate of photon absorption by the actinometer at wavelength of

253.7 nm, Einstein s^{-1}; $A_{ac,253.7}$ being the absorbance of the potassium ferrioxalate solution at wavelength of 253.7 nm.

As $A_{ac,\ 253.7}$ is greater than two during the entire radiation period of the experiments, the amount of light absorbed is greater than 99% of the light received, corresponding to the total absorption of light by the actinometric solution. Eq. (A.3) becomes:

$$P_{ac,253.7} = P_{253.7} \tag{A.4}$$

According to Eq. (A.2), the rate of photon absorption by the potassium ferrioxalate is:

$$P_{ac,253.7} = \frac{N_{ac,253.7}}{t} \tag{A.5}$$

Combining Eqs. (A.2), (A.4) and (A.5) gives the radiation flow rate of lamp $P_{253.7}$:

$$P_{253.7} = \frac{n_{ac}}{\phi_{ac,253.7} t} \tag{A.6}$$

Hence, the radiation flow rate $P_{253.7}$ emitted by the lamp of 30 and 10 W was determined as $(4.47 \pm 0.17) \times 10^{-6}$ and $(2.40 \pm 0.13) \times 10^{-6}$ Einstein s^{-1}, respectively.

References

[1] A.M. Talarposhti, T. Donnelly, G.K. Anderson, Colour removal from a simulated dye wastewater using a two-phase anaerobic packed bed reactor, Water Res. 35 (2001) 425–432.

[2] I. Arslan, A. Bacioglu, Oxidative treatment of simulated dyehouse by UV and near-UV light assisted Fenton's reagent, Chemosphere 39 (1999) 2767–2783.

[3] G.M. Sandra, S.F. Renato, D. Nelson, Degradation and toxicity reduction of textile effluent by combined photocatalytic and ozonation processes, Chemosphere 40 (2000) 369–373.

[4] S. Ledakowicz, M. Solecka, R. Zylla, Biodegradation, decolourisation and detoxification of textile wastewater enhanced by advanced oxidation processes, J. Biotechnol. 89 (2001) 175–184.

[5] W. Chu, C.W. Ma, Reaction kinetics of UV-decolourization for dye materials, Chemosphere 37 (1998) 961–974.

[6] T. Sauer, G.C. Neto, H.J. José, R.F.P.M. Moreira, Kinetics of photocatalytic degradation of reactive dyes in a TiO_2 slurry reactor, J. Photochem. Photobiol. A: Chem. 149 (2002) 147–154.

[7] N. Daneshvar, D. Salari, A.R. Khataee, Photocatalytic degradation of azo dye acid red 14 in water: investigation of the effect of operational parameters, J. Photochem. Photobiol. A: Chem. 157 (2003) 111–116.

[8] I.M. Banat, P. Nigam, D. Singh, R. Marchant, Microbial decolorization of textile-dye-containing effluents: a review, Bioresour. Technol. 58 (1996) 217–227.

[9] S. Nam, V. Renganathan, P.G. Tratnyek, Substituent effects on azo dye oxidation by the Fe^{III}-EDTA–H_2O_2 system, Chemosphere 45 (2001) 59–65.

[10] W. Chu, S.M. Tsui, Photo-sensitization of diazo disperse dye in aqueous acetone, Chemosphere 39 (1999) 1667–1677.

[11] W. Zhao, H. Shi, D. Wang, Kinetics of the reaction between ozone and Cationic Red X-GRL, Chin. J. Chem. Eng. 11 (2003) 388–394.

[12] A.M. Braun, M.T. Maurette, E. Oliveros, Photochemical Technology, Wiley, New York, 1991.

[13] R.H. Perry, D.W. Green, Perry's Chemical Engineers' Handbook, seventh ed., McGraw-Hill, New York, 1997.

[14] O. Legrini, E. Oliveros, A.M. Braun, Photochemical processes for water treatment, Chem. Eng. Sci. 93 (1993) 671–698.

[15] P. Aranyosi, M. Czilik, E. Rémi, G. Parlagh, A. Vig, I. Rusznák, The light stability of azo dyes and azo dyeings IV. Kinetic studies on the role of dissolved oxygen in the photofading of two heterobifunctional azo reactive dyes in aqueous solution, Dyes Pigments 43 (1999) 173–182.

[16] A. Pajares, J. Gianotti, E. Haggi, G. Stettler, F. Amat-Guerri, S. Bertolotti, S. Criado, N.A. García, Visible light-promoted interactions between riboflavin and 3-hydroxypyridine in aqueous solution, Dyes Pigments 41 (1999) 233–239.

[17] S. Yang, H. Tian, H. Xiao, X. Shang, X. Gong, S. Yao, K. Chen, Photodegradation of cyanine and merocyanine dyes, Dyes Pigments 49 (2001) 93–101.

[18] F. Wilkinson, W.P. Helman, A.B. Ross, Quantum yields for the photosensitized formation of the lowest electronically excited singlet state of molecular oxygen singlet oxygen in solution, J. Phys. Chem. Ref. Data 22 (1993) 113–262.

[19] J.S. Miller, D. Olejnik, Photolysis of polycyclic aromatic hydrocarbons in water, Water Res. 35 (2000) 233–243.

[20] P. Neta, R.E. Huie, A.B. Ross, Rate constants for reactions of peroxyl radicals in fluid solutions, J. Phys. Chem. Ref. Data 19 (1990) 413–513.

[21] M. Koch, A. Yediler, D. Lienert, G. Insel, A. Kettrup, Ozonation of hydrolyzed azo dye reactive yellow 84(CI), Chemosphere 46 (2002) 109–113.

[22] C. Selvaraju, A. Sivakumar, P. Ramamurthy, Excited state reactions of acridinedione dyes with onium salts: mechanistic details, J. Photochem. Photobiol. A: Chem. 138 (2001) 213–226.

[23] G.V. Buxton, C.L. Greenstock, W.P. Helman, A.B. Ross, Critical review of rate constants for reactions of hydrated electrons, hydrogen atoms and hydroxyl radicals ($^{\bullet}OH/^{\bullet}O^{-}$) in aqueous solution, J. Phys. Chem. Ref. Data 17 (1988) 514–883.

[24] O.M. Alfano, R.L. Romero, A.E. Cassano, Radiation field modeling in photoreactors. Prat I: Homogeneous media, Chem. Eng. Sci. 41 (1986) 421–444.